DOI 10.2478/ama-2025-0063

SENSORLESS DIRECT TORQUE CONTROLLED INDUCTION MOTOR DRIVE UTILIZING EXTENDED KALMAN FILTERED RF-MRAS

Hau Huu VO*, **Dung Quang NGUYEN***, **Pavel BRANDSTETTER****

*Modeling Evolutionary Algorithms Simulation and Artificial Intelligence, Faculty of Electrical and Electronics Engineering, Ton Duc Thang University, No. 19 Nguyen Huu Tho Street, Tan Hung Ward, Ho Chi Minh City, Vietnam
**Department of Applied Electronics, Faculty of Electrical Engineering and Computer Science, VSB-Technical University of Ostrava, 17.listopadu 15, 70833 Ostrava-Poruba, Czech Republic

vohuuhau@tdtu.edu.vn, nguyenquangdung@tdtu.edu.vn, pavel.brandstetter@vsb.cz

received 30 October 2024, revised 17 September 2025, accepted 24 September 2025

Abstract: In order to achieve high performance of sensorless direct torque controlled induction motor drive at medium and low speed regions in case of Gaussian-noised stator currents, extended Kalman filter is utilized. At first, sensorless control using rotor-flux-based model reference adaptive system is described. Then, extended Kalman filtering that uses full state-space model of the induction motor is employed to obtain estimated stator currents for the sensorless control. Unmeasured rotor fluxes in extended Kalman filtering are computed based on their relationship to estimated stator fluxes and measured stator currents. The estimated stator currents are utilized to compute input quantities for direct torque control. Simulations are deployed in case of both process and measurement noises of stator currents. Performance comparisons based on two indices: normalized integral of time multiplied by absolute value of speed difference and maximum value of absolute value of relative speed difference between two sensorless control methods with and without extended Kalman filter, are carried out. Through simulations in Simulink environment of Matlab software, theoretical assumptions are confirmed by the fact that the evaluation indices of the proposed method are decreased by at most 75% and 80% compared to the method without extended Kalman filter.

Key words: direct torque control, extended Kalman filtering, induction motor, rotor-flux model reference adaptive system, sensorless control

1. INTRODUCTION

Direct torque control (DTC) strategies have been offering high efficiency in AC drive applications [1]-[5]. The DTC integrated pulse width modulation (PWM) was employed to enhance the energy production for a wind turbine drive application using synchronous generator [1]. The PWM-DTC IM drive that contained start process, was presented to ensure favorable transient and constant switching frequency [2]. The DTC with only one PI speed controller and without calculations of sector and rotating frame, was proposed to increase computational speed [3]. The virtual vectors were deployed to lower the torque ripple in a wide speed range [4]. In order to decrease fluctuations flux and torque and to increase the drive stability, the twelve-sector DTC were combined with IM parameter estimation based on model reference adaptive system (MRAS) [5]. Methods of sensorless control and supervision for induction motor (IM) have been interesting topics [6]-[7]. In sensorless drives, MRAS techniques have been widely utilized [8]-[19]. Rotor-flux-based MRAS (RF-MRAS) and stator-current-based MRAS (SC-MRAS) were compared in cases of simultaneous uncertainties of IM parameters [8]. The MRAS was utilized to estimate parameters in sensorless permanent magnet synchronous motor (PMSM) drive [9]. The speed of synchronous reluctance motor (SRM) was estimated by reactive-power-based MRAS [10]. Stator-flux based MRAS was integrated into phase opposition disposition based five-level inverter to increase the parameter estimation accuracy and the IM drive performance [11]. The MRAS was modified to maximize power control and eliminate sensors for PMSM solar pump system [12]. The MRAS estimator was adjusted to observe the flux linkage of an interior PMSM drive system [13].

In case of deterministic observers, various techniques such as fuzzy logic, sliding mode (SM), artificial neural network (ANN), were integrated into the MRAS to obtain higher drive performances [14]-[19]. The MRAS was integrated the fuzzy logic into its adaptation mechanism for sensorless permanent magnet synchronous generator (PMSG) drive [14]. The ANN and particle swarm optimization were combined to improve the performance of the MRAS for sensorless control of an induction generator [15]. The RF-MRAS was enhanced by the integral SM control for sensorless IM drive [16]. In order to increase robustness and performance of sensorless IM drive, discrete SM observer was integrated into the MRAS [17]. The SM observer combined with the MRAS one, provided three types of observers that were enhanced by the sliding mode DTC for the high-performance IM control [18]. The ANN was employed with a variant of the Q-MRAS for sensorless IM drive [19]. For stochastic systems, Kalman filters (KFs) were deployed [20]-[30].

Various industrial applications such as health monitoring, robotics, sensorless control, generation systems were analysed briefly [20]. The KF increased GPS accuracy and reduced magnetometer measurement noise for estimation of position and orientation [21]. Stator currents and their derivatives were smoothed by the KF for sensorless vector controlled IM drive using back-electromotive-force-based MRAS [22]. The extended KF (EKF) provided estimated feedback signal for suspension control system with spiral springs and magnetorheological dampers [23]. Rotor speed, rotor

position and machine parameters of the SRM were estimated by the KF [24]. Speed and rotor flux were computed by the EKF that approximated covariance matrices of noise process and measurement vectors using genetic algorithm [25]. Noise covariance matrices were also adapted for sensorless drive using the EKF that integrated the maximum likelihood criterion and weighting algorithm [26]. An ANN-based observer was trained by the KF to improve the speed response [27]. The EKF was combined with intelligent magnetic model for SRM drive [28]. An iterated EKF that used two IM models was utilized to obtain estimations of IM resistances and speed [29]. The current noise was compensated by the EKF to improve the performance of sensorless PMSM drive using the MRAS [30]. Discretization methods were analyzed and selected for increasing precision of the flux and speed estimations for induction generator [31]. The extended KF that used the suboptimal principle enhanced the robustness in combination with the MRAS for sensorless bearingless IM control [32]. Next section, in order to reduce influence of Gaussian noises of stator currents on sensorless PWM-DTC IM drive using the RF-MRAS and simultaneously improve its estimation accuracy at medium and low speed areas [8], [16], the EKF that utilizes the IM model to obtain smoothed stator currents is presented. The filtered currents are employed for computations of both estimated speed and important quantities of the DTC. The third section is simulations and discussions. Conclusions are carried out in final section.

2. PROPOSED SENSORLESS CONTROL

Figure 1 shows the sensorless DTC IM drive using EKF-based MRAS. Input quantities for the DTC drive are computed according to Eqs. (1)-(5):

$$\psi_{s\alpha,est} = \int \left(u_{s\alpha} - R_s i_{s\alpha,KF}\right) dt \tag{1}$$

$$\psi_{s\beta,est} = \int \left(u_{s\beta} - R_s i_{s\beta,KF}\right) dt \tag{2}$$

$$\psi_{s,est} = \sqrt{\psi_{s\alpha,est}^2 + \psi_{s\beta,est}^2} \tag{3}$$

$$\gamma_{est} = arcsin\left(\frac{\psi_{s\beta,est}}{\psi_{s,est}}\right) \tag{4}$$

$$T_{e,est} = \frac{3n_p\left(i_{s\beta,KF}\psi_{s\alpha,est} - i_{s\alpha,KF}\psi_{s\beta,est}\right)}{2} \tag{5}$$

where, $u_{s\alpha}$, $u_{s\beta}$: stator voltages; $\psi_{s\alpha,est}$ & $\psi_{s\beta,est}$: estimated stator fluxes; γ_{est}: estimated orienting angle; $T_{e,est}$: estimated motor torque; R_s: stator resistance; n_p: number of pole pairs; $i_{s\alpha,KF}$ & $i_{s\beta,KF}$: stator currents filtered by Extended Kalman Filtering block. Discrete state-space IM model that is distorted by zero-mean, Gaussian process & measurement noise vectors $\boldsymbol{v}$ & $\boldsymbol{w}$, is described by Eqs. (6)-(7):

$$\boldsymbol{X}(k+1) = \widehat{\mathbf{A}}_d \boldsymbol{X}(k) + \mathbf{B}_d \boldsymbol{U}(k) + \boldsymbol{v}(k) \tag{6}$$

$$\boldsymbol{Y}(k) = \mathbf{C}_d \boldsymbol{X}(k) + \boldsymbol{w}(k) \tag{7}$$

where

$$\boldsymbol{X} = [i_{s\alpha} \quad i_{s\beta} \quad \psi_{r\alpha} \quad \psi_{r\beta}]^T \tag{8}$$

$$\boldsymbol{U} = [u_{s\alpha} \quad u_{s\beta}]^T \tag{9}$$

$$\widehat{\mathbf{A}}_d = \mathbf{I} + t_d \widehat{\mathbf{A}} \tag{10}$$

$$\widehat{\mathbf{A}} = \begin{bmatrix} c_1 & 0 & c_2 & c_3\widehat{\omega}_r \\ 0 & c_1 & -c_3\widehat{\omega}_r & c_2 \\ \frac{L_m R_r}{L_r} & 0 & -\frac{R_r}{L_r} & -\widehat{\omega}_r \\ 0 & \frac{L_m R_r}{L_r} & \widehat{\omega}_r & -\frac{R_r}{L_r} \end{bmatrix} \tag{11}$$

$$\mathbf{B}_d = t_d \mathbf{B} \tag{12}$$

$$\mathbf{B} = \frac{1}{\sigma L_s}\begin{bmatrix} 1 & 0 & 0 & 0 \\ 0 & 1 & 0 & 0 \end{bmatrix}^T \tag{13}$$

$$\mathbf{C}_d = \begin{bmatrix} 1 & 0 & 0 & 0 \\ 0 & 1 & 0 & 0 \end{bmatrix} \tag{14}$$

$$c_1 = -\frac{L_m^2 R_r + L_r^2 R_s}{\sigma L_s L_r^2} \tag{15}$$

$$c_2 = \frac{L_m R_r}{\sigma L_s L_r^2} \tag{16}$$

$$c_3 = \frac{L_m}{\sigma L_s L_r} \tag{17}$$

$$\sigma = 1 - \frac{L_m^2}{L_s L_r} \tag{18}$$

t_d: discretization period; $i_{s\alpha}$ & $i_{s\beta}$: stator currents; $\psi_{r\alpha}$ & $\psi_{r\beta}$: rotor fluxes; L_s & L_m: stator & magnetizing inductances; R_r & L_r: rotor resistance & rotor inductance.

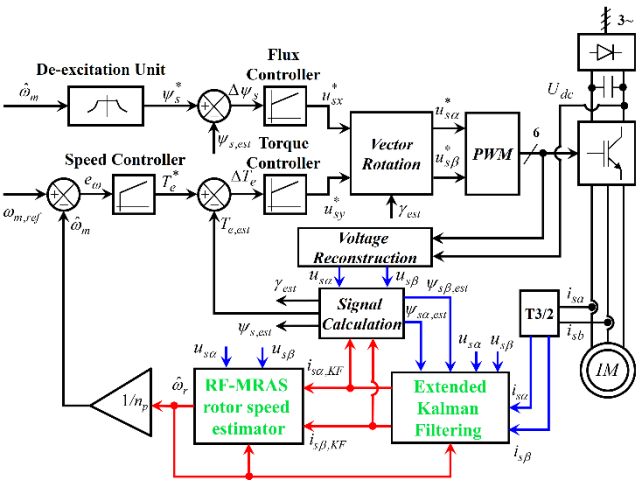

Fig. 1. Sensorless DTC IM drive using KF-based RF-MRAS

The EKF block estimates state vector X_{KF} that contains currents $i_{s\alpha,KF}$ and $i_{s\beta,KF}$ according to Eqs. (19)-(25):

$$\widetilde{\boldsymbol{X}}(k+1) = \widehat{\mathbf{A}}_d \boldsymbol{X}_{KF}(k) + \mathbf{B}_d \boldsymbol{U}(k) \tag{19}$$

$$\widetilde{\mathbf{P}}(k+1) = \widehat{\mathbf{A}}_d \mathbf{P}_{KF}(k) \widehat{\mathbf{A}}_d^T(k) + \mathbf{Q} \tag{20}$$

$$\mathbf{K}(k+1) = \widetilde{\mathbf{P}}(k+1)\mathbf{C}_{d,KF}^T\left[\mathbf{C}_{d,KF}\widetilde{\mathbf{P}}(k+1)\mathbf{C}_{d,KF}^T + \mathbf{R}\right]^{-1} \tag{21}$$

$$\boldsymbol{X}_{KF}(k+1) = \widetilde{\boldsymbol{X}}(k+1) + \mathbf{K}(k+1)\left[\boldsymbol{Y}_m(k) - \widetilde{\boldsymbol{Y}}(k+1)\right] \tag{22}$$

$$\mathbf{P}_{KF}(k+1) = \widetilde{\mathbf{P}}(k+1) - \mathbf{K}(k+1)\mathbf{C}_{d,KF}\widetilde{\mathbf{P}}(k+1) \tag{23}$$

$$\boldsymbol{Y}_m(k) = \mathbf{C}_{d,KF}\, \boldsymbol{X}_m(k) \tag{24}$$

$$\widetilde{\boldsymbol{Y}}(k) = \mathbf{C}_{d,KF}\, \widetilde{\boldsymbol{X}}(k) \tag{25}$$

where

DOI 10.2478/ama-2025-0063

$$\boldsymbol{X}_{KF} = [i_{s\alpha,KF} \quad i_{s\beta,KF} \quad \psi_{r\alpha,KF} \quad \psi_{r\beta,KF}]^T \tag{26}$$

$$\mathbf{C}_{d,KF} = \mathbf{I} \tag{27}$$

$$\boldsymbol{X}_m = \boldsymbol{X} \tag{28}$$

Because rotor fluxes in vector $\boldsymbol{X}_m$ are not measured, they are calculated according to Eqs. (29)-(30) [1]:

$$\psi_{r\alpha} = \frac{L_r}{L_m}\psi_{s\alpha,est} - \frac{1}{c_3}i_{s\alpha} \tag{29}$$

$$\psi_{r\beta} = \frac{L_r}{L_m}\psi_{s\beta,est} - \frac{1}{c_3}i_{s\beta} \tag{30}$$

Symbol ~ represents predicted quantities; letters "*KF*" denote for ones estimated using KF; **Q** & **R**– covariance matrices of ***v*** & ***w*** with, the matrix **R** is assumed to be known; **P** – state vector covariance matrix; **K** – Kalman gain.

For reference model or voltage model [8], rotor fluxes are computed according to Eqs. (31)-(32):

$$\psi_{r\alpha,r} = \frac{L_r}{L_m}\int\left(u_{s\alpha} - R_s i_{s\alpha,KF}\right)dt - \frac{1}{c_3}i_{s\alpha,KF} \tag{31}$$

$$\psi_{r\beta,r} = \frac{L_r}{L_m}\int\left(u_{s\beta} - R_s i_{s\beta,KF}\right)dt - \frac{1}{c_3}i_{s\beta,KF} \tag{32}$$

In case of adaptive model or current model that contains estimated rotor speed $\hat{\omega}_r$, rotor fluxes are calculated by Eqs. (33)-(34):

$$\psi_{r\alpha,a} = \int\left(-\frac{R_r}{L_r}\psi_{r\alpha,a} - \hat{\omega}_r\psi_{r\beta,a} + \frac{L_m R_r}{L_r}i_{s\alpha,KF}\right)dt \tag{33}$$

$$\psi_{r\beta,a} = \int\left(\hat{\omega}_r\psi_{r\alpha,a} - \frac{R_r}{L_r}\psi_{r\beta,a} + \frac{L_m R_r}{L_r}i_{s\beta,KF}\right)dt \tag{34}$$

Thanks to Popov's theorem for minimizing adaptive signal ξ [16], the estimated rotor speed is obtained by Eqs. (35)-(36):

$$\xi = \psi_{r\alpha,a}\psi_{r\beta,r} - \psi_{r\beta,a}\psi_{r\alpha,a} \tag{35}$$

$$\hat{\omega}_r = K_p\xi + K_i\int\xi dt \tag{36}$$

where, $\psi_{r\alpha,r}$ & $\psi_{r\beta,r}$: rotor fluxes of the reference model; $\psi_{r\alpha,a}$ & $\psi_{r\beta,a}$: rotor fluxes of the adaptive model; K_p & K_i: proportional & integral gains.

3. SIMULATIONS AND DISCUSSIONS

Parameters of the IM are given in Table 1. Simulations of two sensorless RF-MRAS-based DTC IM drives: the first one is without extended Kalman filtering and the second one is with extended Kalman filtering (abbreviated as NK and KF in the rest of the text), are implemented at variances of Gaussian system and measurement noises of stator currents $\delta_p^2 = \{0.1^2, 0.5^2, 1.0^2\}$ and $\delta_m^2 = \{0.1^2, 0.5^2, 1.0^2\}$. Proportional gains and integral time constants of the speed, flux, torque controllers & the rotor speed estimator are {1.5, 100, 5 & 500} and {0.05s, 0.01s, 0.05s & 0.002s}. Diagram of load torque is identical to the one, and reference speed course is similar to one $\omega_{m,ref} = \{5\pi/3$ rad/s, 10π rad/s } [16]. The utilized PWM technique is space vector one with switching frequency of 20kHz, inverter DC link of 540Vdc. Normalized integral of time multiply by absolute value of speed difference ($ITAE_n$) [16] is used to assess two sensorless drives according to Eq. (37):

$$ITAE_n = \frac{\int_0^2 t|e_\omega(t)|dt}{max|\omega_{m,ref}|} \tag{37}$$

Tab. 1. Induction motor parameters

Symbol	Quantity	Value
R_s	Stator resistance	3.179Ω
n_p	Number of pole pairs	2
$L_s = L_r$	Stator & rotor inductances	0.209H
L_m	Magnetizing inductance	0.192H
R_r	Rotor resistance	2.118Ω
P_n	Rated power	2200W
$\omega_{m,n}$	Rated speed	142π/3 rad/s
$T_{e,n}$	Rated torque	14.8N·m
J_m	Moment of inertia	0.0047kg·m^2

Figures 2-4, 5-7 respectively show motor speed responses in cases of $\delta_p^2 = \delta_m^2$ at $\omega_{m,ref} = 5\pi/3$ rad/s, $\omega_{m,ref} = 10\pi$ rad/s. The figures indicate that as the variance increases, the performance of the speed response is improved more. Tables 2 and 3 list the $ITAE_n$ at $\omega_{m,ref} = 5\pi/3$ rad/s and $\omega_{m,ref} = 10\pi$ rad/s in all cases of variances. The tables show that the ratio ($ITAE_{n,KF}/ITAE_{n,NF}$) is smallest when the ratio (δ_m^2/δ_p^2) is largest, and vice versa (see Figs. 8-9). The ratios ($ITAE_{n,KF}/ITAE_{n,NF}$) are in ranges of [24.2%; 98.9%], [24.6%; 99.0%] for $\omega_{m,ref} = 5\pi/3$ rad/s, $\omega_{m,ref} = 10\pi$ rad/s, respectively.

Time courses of relative speed difference RSD ($e_\omega/\max|\omega_{m,ref}|$) for cases of the ratio ($ITAE_{n,KF}/ITAE_{n,NF}$) reach maximum & minimum at $\omega_{m,ref} = 5\pi/3$ rad/s and $\omega_{m,ref} = 10\pi$ rad/s are respectively shown in Figs. 10 and 11. Diagrams of stator currents are displayed in Figs. 12-13 and 14-15 for $\omega_{m,ref} = 5\pi/3$ rad/s and $\omega_{m,ref} = 10\pi$ rad/s, respectively. The reason why the proposed EKF-based MRAS speed estimator is more efficient in the cases of larger ratio (δ_m^2/δ_p^2), is because the matrix **R** is assumed to be known. The covariance matrices **Q** and **R** can be estimated according to the methods in [25]-[26]. Quantities including stator fluxes, rotor fluxes of reference model, rotor fluxes of adaptive model, and adaptive signal at $\omega_{m,ref} = 5\pi/3$ rad/s & $\omega_{m,ref} = 10\pi$ rad/s, $\delta_p^2=0.1^2$, $\delta_m^2=1^2$ are respectively presented in Figs. 16-17, 18-19, 20-21, and 22-23. Figures 22-23 indicate that ripple of the adaptive signal for the KF is much smaller than that for the NF. This results in significantly lower *RSD* for the KF. Tables 4-5 show maximum value of absolute of relative speed difference (*MARSD*) at $\omega_{m,ref} = 5\pi/3$ rad/s & $\omega_{m,ref} = 10\pi$ rad/s for all variances. The *MARSD* is reduced by 80% and 77% at most, corresponding to $\delta_p^2=0.1^2$, $\delta_m^2=1^2$, for $\omega_{m,ref} = 5\pi/3$ rad/s and $\omega_{m,ref} = 10\pi$ rad/s, respectively.

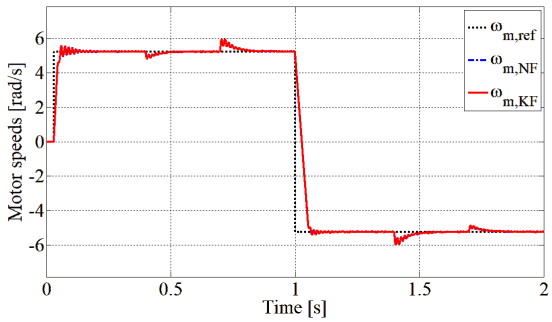

Fig. 2. Motor speeds at $\omega_{m,ref} = 5\pi/3$ rad/s, $\delta_p^2=\delta_m^2=0.1^2$.

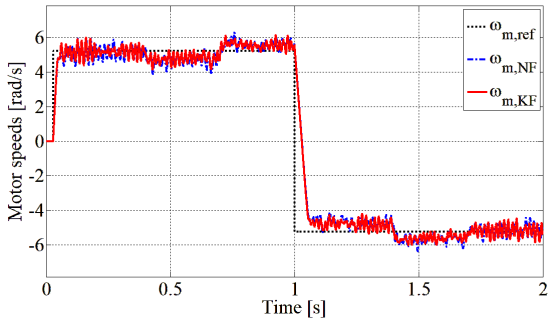

Fig. 3. Motor speeds at $\omega_{m,ref}$ = 5π/3 rad/s, $\delta_p^2=\delta_m^2=0.5^2$

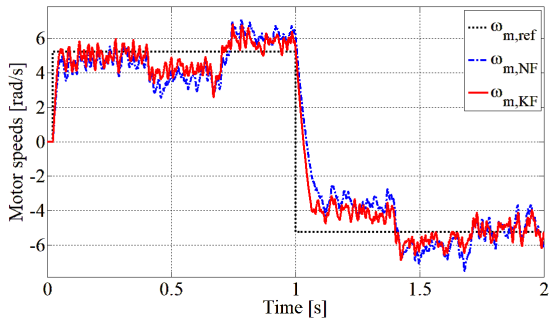

Fig. 4. Motor speeds at $\omega_{m,ref}$ = 5π/3 rad/s, $\delta_p^2=\delta_m^2=1^2$

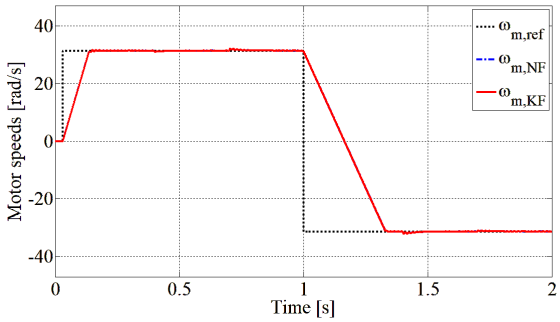

Fig. 5. Motor speeds at $\omega_{m,ref}$ = 10π rad/s, $\delta_p^2=\delta_m^2=0.1^2$

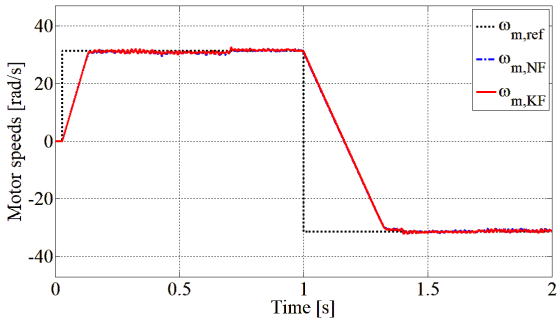

Fig. 6. Motor speeds at $\omega_{m,ref}$ = 10π rad/s, $\delta_p^2=\delta_m^2=0.5^2$

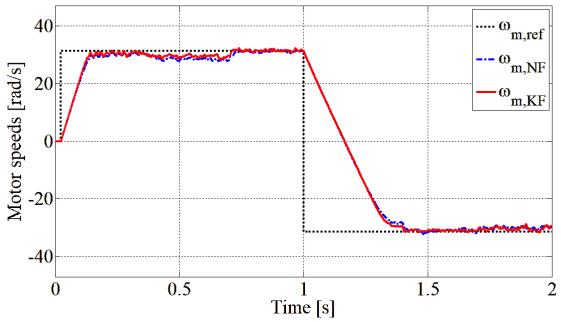

Fig. 7. Motor speeds at $\omega_{m,ref}$ = 10π rad/s, $\delta_p^2=\delta_m^2=1^2$

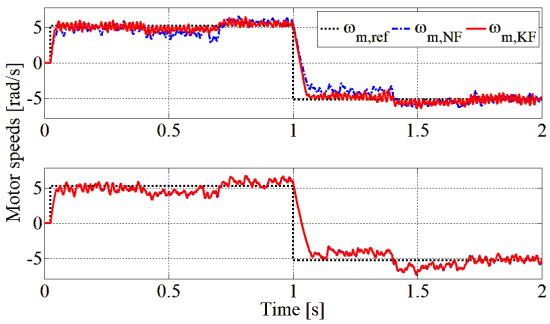

Fig. 8. Motor speeds at $\omega_{m,ref}$ = 5π/3 rad/s: case 1 (upper): $\delta_p^2=0.1^2$, $\delta_m^2=1^2$ and case 2 (lower): $\delta_p^2=1^2$, $\delta_m^2=0.1^2$

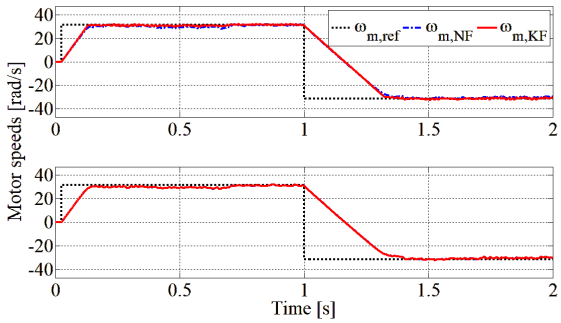

Fig. 9. Motor speeds at $\omega_{m,ref}$ = 10π rad/s: case 1 (upper): $\delta_p^2=0.1^2$, $\delta_m^2=1^2$ and case 2 (lower): $\delta_p^2=1^2$, $\delta_m^2=0.1^2$

Tab. 2. $ITAE_n \times 10^{-2}$ [s²] at $\omega_{m,ref}$ = 5π/3 rad/s

δ_p^2	δ_m^2 = 0.1²		δ_m^2 = 0.5²		δ_m^2 = 1.0²	
	NF	KF	NF	KF	NF	KF
0.1²	3.13	2.46	47.0	16.0	185	44.7
0.5²	47.1	45.4	65.8	44.8	191	94.6
1.0²	185	183	191	160	262	175

Tab. 3. $ITAE_n \times 10^{-2}$ [s²] at $\omega_{m,ref}$ = 10π rad/s

δ_p^2	δ_m^2 = 0.1²		δ_m^2 = 0.5²		δ_m^2 = 1.0²	
	NF	KF	NF	KF	NF	KF
0.1²	0.59	0.49	7.84	2.78	30.6	7.53
0.5²	7.80	7.53	10.9	7.41	31.6	15.6
1.0²	30.6	30.3	31.5	26.5	43.3	28.9

DOI 10.2478/ama-2025-0063

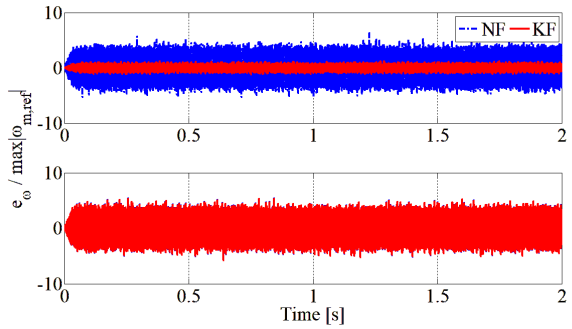

Fig. 10. RSD at $\omega_{m,ref}$ = 5π/3 rad/s: case 1 (upper): δ_p^2=0.1², δ_m^2=1² and case 2 (lower): δ_p^2=1², δ_m^2=0.1²

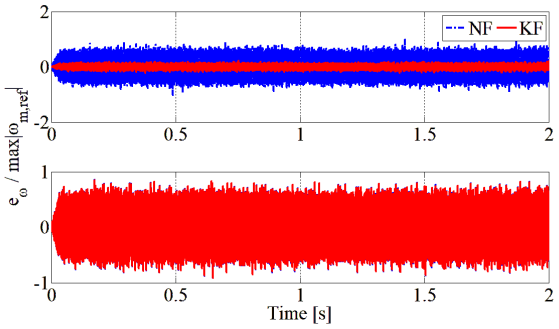

Fig. 11. RSD at $\omega_{m,ref}$ = 10π rad/s: case 1 (upper): δ_p^2=0.1², δ_m^2=1² and case 2 (lower): δ_p^2=1², δ_m^2=0.1²

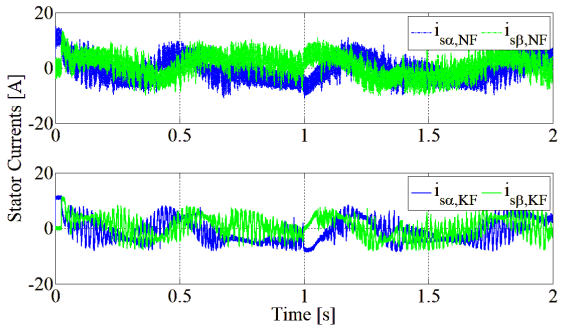

Fig. 12. Stator currents at $\omega_{m,ref}$ = 5π/3 rad/s, δ_p^2=0.1², δ_m^2=1²

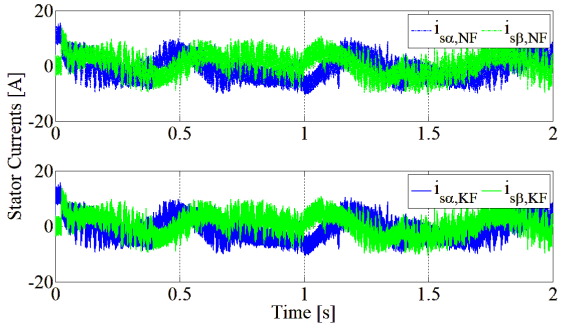

Fig. 13. Stator currents at $\omega_{m,ref}$ = 5π/3 rad/s, δ_p^2=1², δ_m^2=0.1²

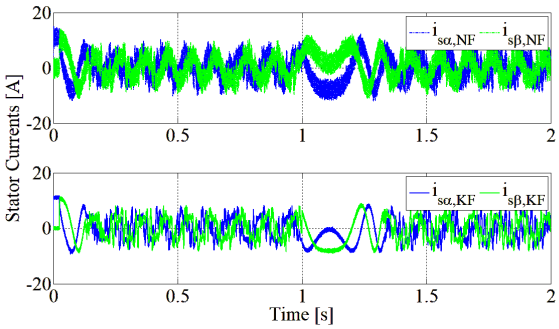

Fig. 14. Stator currents at $\omega_{m,ref}$ = 10π rad/s, δ_p^2=0.1², δ_m^2=1²

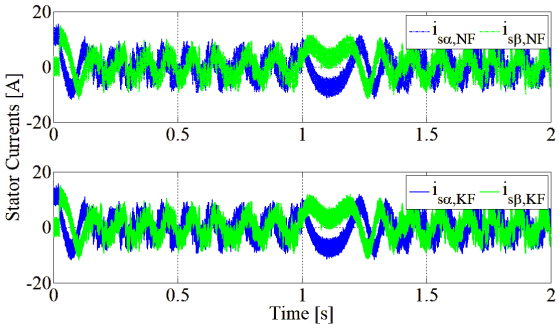

Fig. 15. Stator currents at $\omega_{m,ref}$ = 10π rad/s, δ_p^2=1², δ_m^2=0.1²

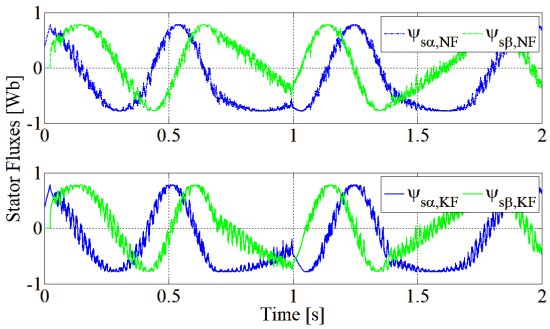

Fig. 16. Stator fluxes at $\omega_{m,ref}$ = 5π/3 rad/s, δ_p^2=0.1², δ_m^2=1²

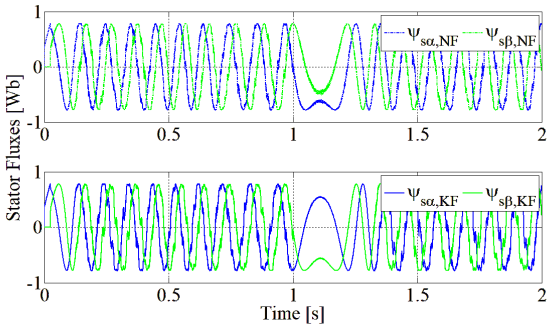

Fig. 17. Stator fluxes at $\omega_{m,ref}$ = 10π rad/s, δ_p^2=0.1², δ_m^2=1²

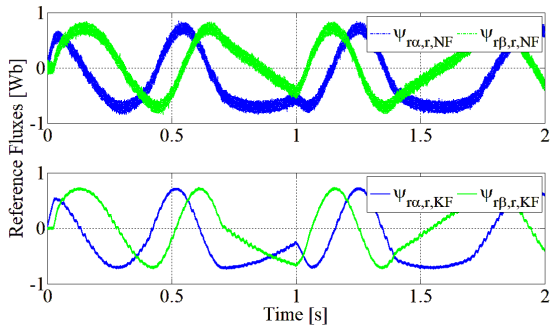

Fig. 18. Rotor fluxes of reference model at $\omega_{m,ref}$ = 5π/3 rad/s, δ_p^2=0.1², δ_m^2=1²

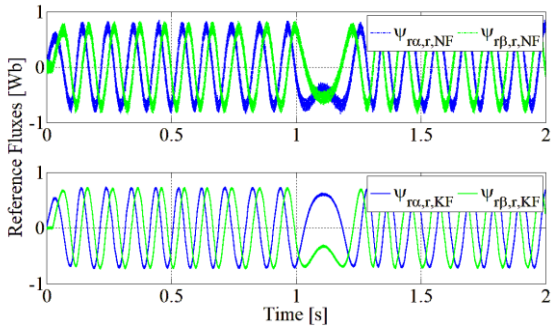

Fig. 19. Rotor fluxes of reference model at $\omega_{m,ref}$ = 10π rad/s, δ_p^2=0.1², δ_m^2=1²

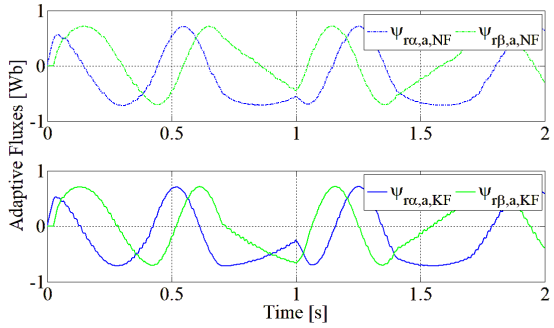

Fig. 20. Rotor fluxes of the adaptive model at $\omega_{m,ref}$ = 5π/3 rad/s, δ_p^2=0.1², δ_m^2=1²

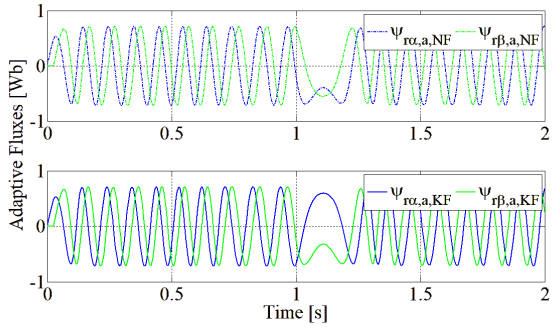

Fig. 21. Rotor fluxes of the adaptive model at $\omega_{m,ref}$ = 10π rad/s, δ_p^2=0.1², δ_m^2=1²

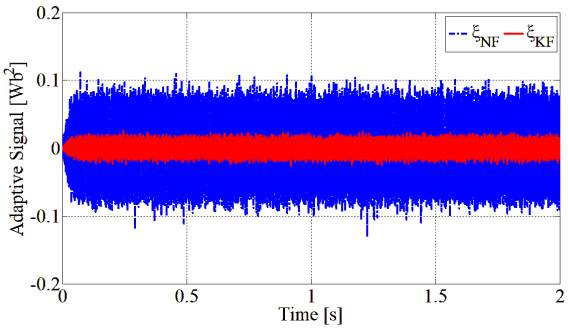

Fig. 22. Adaptive sginal at $\omega_{m,ref}$ = 5π/3 rad/s, δ_p^2=0.1², δ_m^2=1²

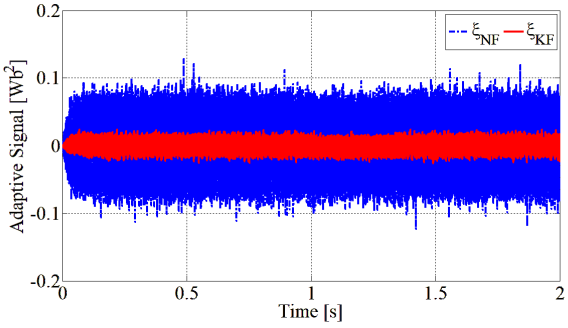

Fig. 23. Adaptive sginal at $\omega_{m,ref}$ = 10π rad/s, δ_p^2=0.1², δ_m^2=1²

Tab. 4. MARSD at $\omega_{m,ref}$ = 5π/3 rad/s

δ_p^2	δ_m^2 = 0.1²		δ_m^2 = 0.5²		δ_m^2 = 1.0²	
	NF	KF	NF	KF	NF	KF
0.1²	0.18	0.17	1.54	0.47	6.30	1.26
0.5²	1.46	1.40	2.07	1.38	6.03	2.99
1.0²	5.81	5.75	5.85	4.78	7.85	5.54

Tab. 5. MARSD at $\omega_{m,ref}$ = 10π rad/s

δ_p^2	δ_m^2 = 0.1²		δ_m^2 = 0.5²		δ_m^2 = 1.0²	
	NF	KF	NF	KF	NF	KF
0.1²	0.03	0.03	0.27	0.08	1.02	0.23
0.5²	0.23	0.22	0.35	0.26	1.08	0.52
1.0²	0.93	0.92	0.94	0.79	1.36	0.91

4. CONCLUSIONS

Sensorless RF-MRAS drives without EKF and with EKF were presented and simulated in cases of process and measurement noises of stator currents. The sensorless drive utilizing the EKF, reduces the ITAEn and MARSD compared to the one without using EKF, especially up to 75% and 80% in cases where the ratio between measurement noise variance and process noise variances is maximum at simulated lower reference speed. In case of the stochastic systems, the method can be employed for other MRAS-based speed estimators that use stator current as inputs. For the SM-based MRASs such as [16]-[18], it can be integrated to estimate components of stator flux and rotor flux vectors at the low and medium speed ranges of the time courses. Because the proposed sensorless control uses the full IM model in the EKF block, the calculation process is slow. Other Kalman Filter versions or estimation techniques of covariance matrices can be deployed to enhance the sensorless drive performance and increase computation speed.

REFERENCES

1. Youness EM, Aziz D, Abdelaziz EG, Najib EO, Othmane Z. DTC-SVM Control for permanent magnet synchronous generator based variable speed wind turbine. International Journal of Power Electronics and Drive Systems. 2017; 8(4): 1732-1743. https://doi.org/10.11591/ijpeds.v8i4.pp1732-1743
2. Brandstetter P, Kuchar M, Vo HH, Dong CST. Induction motor drive with PWM direct torque control. Proceedings of the 2017 18th International Scientific Conference on Electric Power Engineering (EPE). 2017; 409-413. https://doi.org/10.1109/EPE.2017.7967268
3. Peter AK, Mathew J, Gopakumar K. A Simplified DTC-SVPWM Scheme for Induction Motor Drives Using a Single PI Controller. IEEE Transactions on Power Electronics. 2023; 38(1): 750-761. https://doi.org/10.1109/TPEL.2022.3197362
4. Shao B, Zhu ZQ, Yan L, Feng J, Guo S, Li Y, Feng L. Torque Ripple Reduction for Direct Torque Control of Dual Three-Phase PMSM Based on Multiple Virtual Voltage Vectors. IEEE Transactions on Energy Conversion. 2023; 38(1): 296-309. https://doi.org/10.1109/TEC.2022.3208784
5. Ouanjli NE, Mahfoud S, Al-Sumaiti AS, Daoudi SE, Derouich A, Mahfoud ME, Mossa MA. Improved twelve sectors DTC strategy of induction motor drive using Backstepping speed controller and P-MRAS stator resistance identification-design and validation. Alexandria Engineering Journal. 2023; 80: 358-371. https://doi.org/10.1016/j.aej.2023.08.077
6. Bose BK. Modern Power Electronics and AC Drives. Upper Saddle River. New Jersey USA. Prentice Hall; 2002.
7. Bellahsene NRH. Fuzzy Based Supervision Approach in the Event of Rotational Speed Inversion in an Induction Motor. Acta Mechanica et Automatica. 2024; 18(1): 68-76. https://doi.org/10.2478/ama-2024-0009
8. Vo HH, Brandstetter P, Tran TC, Dong CST. An Implementation of Rotor Speed Observer for Sensorless Induction Motor Drive in Case of Machine Parameter Uncertainty. Advances in Electrical and Electronic Engineering. 2018; 16(4): 426-434. https://doi.org/10.15598/aeee.v16i4.2973
9. Kivanc OC, Ozturk SB. Sensorless PMSM Drive Based on Stator Feedforward Voltage Estimation Improved With MRAS Multiparameter Estimation. IEEE/ASME Transactions on Mechatronics. 2018; 23(3): 1326-1337. https://doi.org/ 10.1109/TMECH.2018.2817246.
10. Kumar R, Verma V, Khan YA, Shiva BS. Q-MRAS based Speed Sensorless Vector Controlled Synchronous Reluctance Motor Drive. 2019 International Conference on Power Electronics Applications and Technology in Present Energy Scenario (PETPES), Mangalore, India. 2019: 1-6. https://doi.org/ 10.1109/PETPES47060.2019.9003988.
11. El Daoudi S, Lazrak L, Ouanjli EN, Lafkih MA. Improved DTC-SPWM strategy of induction motor by using five-level POD-PWM inverter and MRASSF estimator. International Journal of Dynamics and Control. 2021; 9(2): 448-462. https://doi.org/10.1007/s40435-020-00667-2
12. Kashif M, Singh B. Modified Active-Power MRAS Based Adaptive Control With Reduced Sensors for PMSM Operated Solar Water Pump. IEEE Transactions on Energy Conversion. 2023; 38(1): 38-52. https://doi.org/10.1109/TEC.2022.3197564
13. Li Z, Yang X, Zhao S. Flux Linkage Observation Using an Improved MRAS Observer in Case of Uniform Demagnetization of IPMSM. IEEE Transactions on Instrumentation and Measurement. 2024; 73: 3508410. https://doi.org/10.1109/TIM.2024.3350109
14. Soufyane B, Abdelhamid R, Smail Z. Signed-Distance Fuzzy Logic Controller Adaptation Mechanism based MRAS Observer for Direct-Drive PMSG Wind Turbines Sensorless Control. 2020 American Control Conference (ACC). Denver CO USA. 2020; 4083-4089. https://doi.org/10.23919/ACC45564.2020.9147811
15. Lakhdar S, Ferroudji F, Roummani K, Koussa K. Enhanced Sensor-Less Control of DFIG-Based Generators Using Hybrid MRAS-ANN Observer and PSO Parameter Optimization. 2023 14th International Renewable Energy Congress (IREC). Sousse. Tunisia. 2023; 1-6. https://doi.org/10.1109/IREC59750.2023.10389203
16. Vo HH. Sensorless Induction Motor Drive Using Modified Integral Sliding Mode Control-Based MRAS. Control Engineering and Applied Informatics. 2023;25(3): 45-54. https://doi.org/10.61416/ceai.v25i3.8563
17. Wang T, Wang B, Yu Y, Xu D. Discrete Sliding-Mode-Based MRAS for Speed-Sensorless Induction Motor Drives in the High-Speed Range. IEEE Transactions on Power Electronics. 2023;38(5):5777-5790. https://doi.org/10.1109/TPEL.2023.3236024
18. Daoudi SE, Lazrak L, Ouanjli NE. New contributions for speed observation of asynchronous motor fed by multilevel inverter. Australian Journal of Electrical and Electronics Engineering. 2023; 20(3): 279-290. https://doi.org/10.1080/1448837X.2023.2191830
19. Kubatko M, Kirschner S, Sotola V, Hamani K, Kuchar M. Sensorless Induction Motor Drive Based on Reactive Power MRAS Estimator Using Artificial Neural Network. 2024 24th International Scientific Conference on Electric Power Engineering (EPE). Kouty nad Desnou. Czech Republic. 2024; 1-4. https://doi.org/ 10.1109/EPE61521.2024.10559577
20. Auger F, Hilairet M, Guerrero JM, Monmasson E, Orlowska-Kowalska T, Katsura S. Industrial Applications of the Kalman Filter: A Review. IEEE Transactions on Industrial Electronics. 2013; 60(12): 5458-5471. https://doi.org/10.1109/TIE.2012.2236994
21. Romaniuk S, Gosiewski Z. Kalman Filter Realization for Orientation and Position Estimation on Dedicated Processor. Acta Mechanica et Automatica. 2014;8(2):88-94. https://doi.org/10.2478/ama-2014-0016
22. Brandstetter P, Dobrovsky M, Kuchar M, Dong CST, Vo HH. Application of BEMF-MRAS with Kalman Filter in Sensorless Control of Induction Motor Drive. Electrical Engineering. 2017;99(4):1151-1160. https://doi.org/10.1007/s00202-017-0613-4
23. Jurkiewicz A, Kowal J, Zajac K. Sky-Hook Control and Kalman Filtering in Nonlinear Model of Tracked Vehicle Suspension System. Acta Mechanica et Automatica. 2017;11(3):222-228. https://doi.org/ 10.1515/ama-2017-0034
24. Mynar Z, Vaclavek P, Blaha P. Synchronous Reluctance Motor Parameter and State Estimation Using Extended Kalman Filter and Current Derivative Measurement. IEEE Transactions on Industrial Electronics. 2021;68(3):1972-1981. https://doi.org/10.1109/TIE.2020.2973897
25. Jayaramu ML, Suresh HN, Bhaskar MS, Almakhles D, Padmanaban S, Subramaniam U. Real-Time Implementation of Extended Kalman Filter Observer With Improved Speed Estimation for Sensorless Control. IEEE Access. 2021; 9: 50452-50465. https://doi.org/10.1109/ACCESS.2021.3069676
26. Tian L, Li Z, Wang Z, Sun X, Guo T, Zhang H. Speed-sensorless control of induction motors based on adaptive EKF. Journal of Power Electronics. 2021;21(12):1823-1833. https://doi.org/10.1007/s43236-021-00325-6
27. Syamkumar U, Jayanand B. A Smoothed Kalman filter Trained MRAS Based Recurrent Neural Observer for Indirect Vector Controlled Induction Motor Drive. 2021 IEEE International Conference on Automatic Control & Intelligent Systems (I2CACIS). Shah Alam. Malaysia. 2021; 396-401. https://doi.org/10.1109/I2CACIS52118.2021.9495860
28. Pasqualotto D, Rigon S, Zigliotto M. Sensorless Speed Control of Synchronous Reluctance Motor Drives Based on Extended Kalman Filter and Neural Magnetic Model. IEEE Transactions on Industrial Electronics. 2023; 70(2): 1321-1330. https://doi.org/10.1109/TIE.2022.3159962
29. Moaveni B, Masoumi Z, Rahmani P. Introducing Improved Iterated Extended Kalman Filter (IIEKF) to Estimate the Rotor Rotational Speed, Rotor and Stator Resistances of Induction Motors. IEEE Access. 2023;11:17584-17593. https://doi.org/10.1109/ACCESS.2023.3244830
30. Cao Y, Ren X, Guo Q, Wu G, Long Q, Ran M. Position Sensorless Control of PMSM Based on EKF Current Noise Compensation and MRAS. 2024 IEEE International Conference on Mechatronics and Automation (ICMA). Tianjin. China. 2024;870-875. https://doi.org/ 10.1109/ICMA61710.2024.10632984

31. Boussoufa A, Ahriche A, Kidouche M, Doghmane MZ. Discretization Order Influences on Extended Kalman Filter Estimation for Doubly-Fed Induction Generator. Przeglad Elektrotechniczny. 2024;100(2): 102-108. https://doi.org/10.15199/48.2024.02.20
32. Bian Y, Yang Z, Sun X, Wang X. Speed Sensorless Control of a Bearingless Induction Motor Based on Modified Robust Kalman Filter. Journal of Electrical Engineering & Technology. 2024;19(3):1179-1190. https://doi.org/10.1007/s42835-023-01649-y

Hau Huu Vo: https://orcid.org/0000-0002-0904-307X

Dung Quang Nguyen: https://orcid.org/0000-0002-4476-6556

Pavel Brandstetter: https://orcid.org/0000-0002-6742-7282